ELSEVIER

Cement & Concrete Composites 22 (2000) 97–113

Cement & Concrete Composites

The nature of the hydration products in hardened cement pastes

I.G. Richardson *

Civil Engineering Materials Unit, School of Civil Engineering, University of Leeds, Leeds LS2 9JT, UK

Received 28 March 1998; accepted 24 September 1999

Abstract

An understanding of the performance of portland cement-based materials requires knowledge at the microstructural level. Developments in the instrumentation of several techniques have led to improved understanding of the composition, morphology, and spatial distribution of the various products of cement hydration. In particular, our understanding of the nature of the nearly amorphous calcium silicate hydrate (C–S–H) phases – which are the principal binding phases in all portland cement-based systems – has been advanced by developments in solid-state NMR spectroscopy and analytical TEM. This paper presents an overview of the nature of the hydration products formed in hardened portland cement-based systems. It starts with the most straightforward cementitious calcium silicate systems, C_3S and β-C_2S, and then considers ordinary portland cement and blends of portland cement with silica fume, ground granulated iron blast-furnace slag, and finally alkali hydroxide-activated slag cements. © 2000 Elsevier Science Ltd. All rights reserved.

Keywords: Blast-furnace slag; C–S–H structure; Capillary porosity; Cement blends; Durability; Microanalysis; Microstructure; NMR; Portland cement; Silica fume; TEM

1. Introduction

An understanding of the performance of portland cement-based materials requires knowledge at the microstructural level: this paper presents an overview of the nature of the hydration products formed in hardened portland cement-based systems; their composition, morphology and spatial distribution. The discussion starts with the most straightforward cementitious calcium silicate systems, C_3S and β-C_2S, and then considers ordinary portland cement and blends of portland cement with silica fume, ground granulated iron blast-furnace slag, and alkali-hydroxide activated slag cements. The paper necessarily draws heavily on previously published work but it contains many new data.

2. Experimental

2.1. Materials

The tricalcium silicate (C_3S) used in the work was prepared by the method of Groves et al. [1] and the β-C_2S was prepared by Rodger [2]. Two portland cements were used: an ordinary portland cement [3], and a white portland cement (from the Aalborg company; Bogue composition (wt%) 65% C_3S, 22% C_2S, 4% C_3A, 1% C_4AF). The latter was needed for the NMR work because of its low Fe content; the presence of paramagnetic ions causes peak broadening in NMR. Various commercial blast-furnace slags (supplied by the Frodingham Cement Company and the AEA Technology Harwell Laboratory) with different chemical and mineralogical compositions and a synthetic slag-glass (AG) were used; chemical data for the glassy phase present in the slags and fineness data are given in Table 1. Powder X-ray diffraction showed that slags SC, HG and VL were >95% glassy whilst slags SM, PT and CP had varying amounts of merwinite and/or melilite.

2.2. Specimen preparation and experimental details

The C_3S, β–C_2S, ordinary portland cement, and portland cement-slag blends were prepared by mixing the required amounts of solids with de-ionized water at a W/S of 0.4; the slurry was then placed in plastic tubes

* Tel.: +44-0113-233-2331; fax: +44-0113-233-2265.
E-mail address: i.g.richardson@leeds.ac.uk (I.G. Richardson).

0958-9465/00/$ - see front matter © 2000 Elsevier Science Ltd. All rights reserved.
PII: S0958-9465(99)00036-0

Table 1
Granulated blast-furnace slags:glass composition (determined by wavelength dispersive X-ray analysis) and fineness data[a]

	SC	SC2	HG	VL	SM	PT	CP	AG
Ca/Si	1.10	1.07	1.21	1.21	1.35	1.17	1.28	1.09
Al/Si	0.36	0.36	0.62	0.40	0.45	0.43	0.36	0.33
Mg/Si	0.32	0.32	0.53	0.44	0.44	0.33	0.05	0.30
n	0.99	–	0.99	0.89	0.97	0.97	0.94	1.01
x_0 μm	22.9	–	17.1	17.5	19.9	27.0	21.6	36.7
Median	16.9	89.3	11.7	9.7	14.0	20.6	13.8	27.1

[a] n and x_0 represent the particle size distribution (Rosin–Rammler constants): n is a measure of breadth of distribution (higher $n \rightarrow$ narrower); x_0 is a measure of average size (36.8% of particles are $> x_0$ μm).

which were sealed in plastic bags before placing in cure baths set at 20°C (C_3S, ordinary cement–slag blends) or 25°C (β-C_2S, white cement–slag blends). The white cement–slag blends and neat commercial slags which were activated with KOH solution were mixed at a S/S of 0.5 and 0.4 respectively. Freshly ground samples were used for X-ray diffraction and NMR. For thermal analysis they were crushed, washed in propan-2-ol, filtered, and stored in a vacuum desiccator prior to analysis. Details of sample preparation and experimental procedures for analytical transmission electron microscopy (TEM) and for X-ray mapping in an electron microprobe analyser (EMPA) are given elsewhere [1,3]. Specimens for nuclear magnetic resonance (NMR) spectroscopy were ground to a powder and packed into zirconia rotors. The single-pulse ^{29}Si spectra for KOH-activated slags HG, SM, PT and CP were acquired using a Bruker MSL-400 spectrometer (magnetic field 9.4 T; operating frequency of 79.49 MHz for ^{29}Si), and slag VL using a Bruker MSL-300 spectrometer (magnetic field 7.1 T; operating frequency of 59.62 MHz for ^{29}Si). All other single-pulse ^{29}Si and ^{1}H–^{29}Si cross polarization (CP) spectra were acquired using a Bruker MSL-200 spectrometer (magnetic field 4.7 T; operating frequencies of 200.13 MHz for ^{1}H and 39.76 MHz for ^{29}Si). The single pulse spectra were acquired over 4000–42,000 scans using flip angles (30–45°) and pulse recycle delays (2–20 s) sufficient to minimize saturation effects. For CP, the Hartmann–Hahn condition was set using kaolinite [4]. ^{29}Si chemical shifts are given relative to tetramethylsilane (TMS) at 0 ppm, with kaolinite used as an external standard at −91.2 ppm. All spectra were apodized with 10 Hz of exponential line broadening and zero filled to 8192 points prior to Fourier transformation. The spectra were iteratively fitted to voigt line shapes using the software Igor [5] with additional macros written by Brough [6]. The full procedure for deconvolution of the white portland cement–slag blends is given by Richardson and Groves [7].

3. Results and discussion

3.1. Reference microstructure

The products of the hydration of tricalcium silicate (C_3S) can be designated as either outer (Op) or inner (Ip) products; outer products form in the originally water-filled spaces and inner products within the boundaries of the original C_3S grains. There is not necessarily an exact correspondence between the positions of the outer boundaries of Ip and the original grains [8]. As alite (impure C_3S) is the most abundant mineral in ordinary portland cement this scheme serves as a convenient reference microstructure for all portland cement-based hardened cement pastes and shall be used in this paper.

3.1.1. C_3S and β-C_2S

The hydration reactions of both C_3S and β-C_2S produce a nearly amorphous C–S–H phase and calcium hydroxide (CH). The CH often occurs as massive crystals but is also mixed with C–S–H at the micron-scale. Fig. 1 shows a Si/Ca atom ratio frequency histogram for the EMPA mapping data from a 70×70 μm region (1 μm increments) in a C_3S paste hydrated for $3\frac{1}{2}$ yr. The region is dominated by one hydrated C_3S grain. Some of the analyses correspond to essentially pure C–S–H, with an average Ca/Si of ≈1.65, and others to admixture of C–S–H with CH. Microanalysis in the TEM – which gives compositions for C–S–H free of admixture with other phases – has shown that the average Ca/Si ratio of the C–S–H phases present in hardened C_3S, β-C_2S, and in ordinary portland cement pastes is always ≈1.7–1.8, Fig. 2 (top); there is no significant variation in Ca/Si with age [3]. There is, however, significant variation at the micron- and nanometre-scale; indeed the Ca/Si ratio of C–S–H in young ordinary portland cement pastes displays a bimodal distribution which becomes unimodal as the pastes mature [3].

In hardened C_3S pastes Op C–S–H has a fibrillar, directional morphology which is a function of space constraint: where it forms in large pore spaces, the fibrils

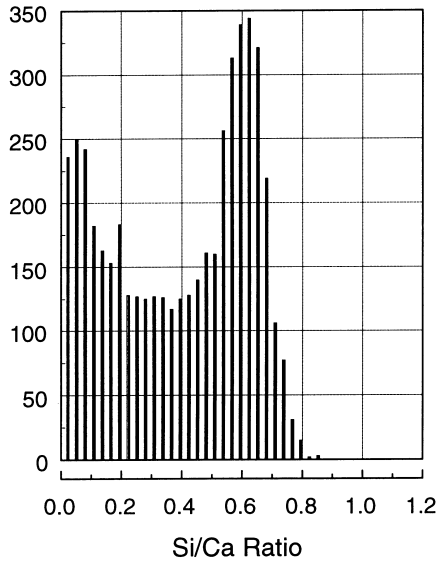

Fig. 1. Si/Ca atom ratio frequency histogram from the mapping data for a 70×70 μm^2 region (1 μm increments) in a C_3S paste hydrated for $3\frac{1}{2}$ yr.

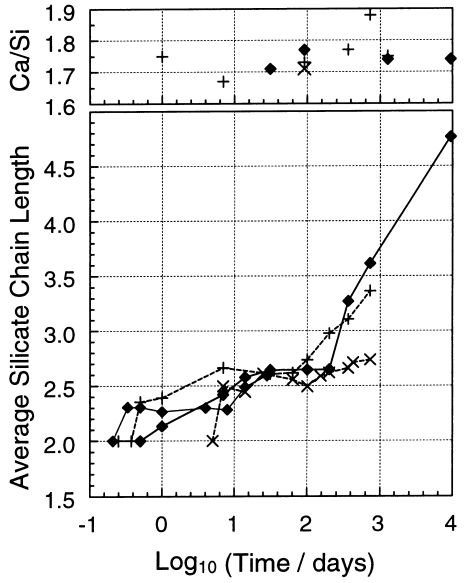

Fig. 2. Ca/Si ratio (top) (from microanalysis in the TEM) and average silicate chain length (from NMR) against hydration time for C–S–H in C_3S (◆), β-C_2S (×) (stabilized with 0.5% Cr), and ordinary portland cement (+) pastes.

form with a high aspect ratio ('coarse fibrillar'); in smaller spaces, it retains a directional aspect but forms in a more space-efficient manner ('fine fibrillar'). The spaces between the fibrils of Op C–S–H form a three-dimensional interconnected pore network – the capillary porosity – which is of major importance for durability. Ip C–S–H has a compact, fine-scale and homogeneous morphology, with only gel porosity – pores within the

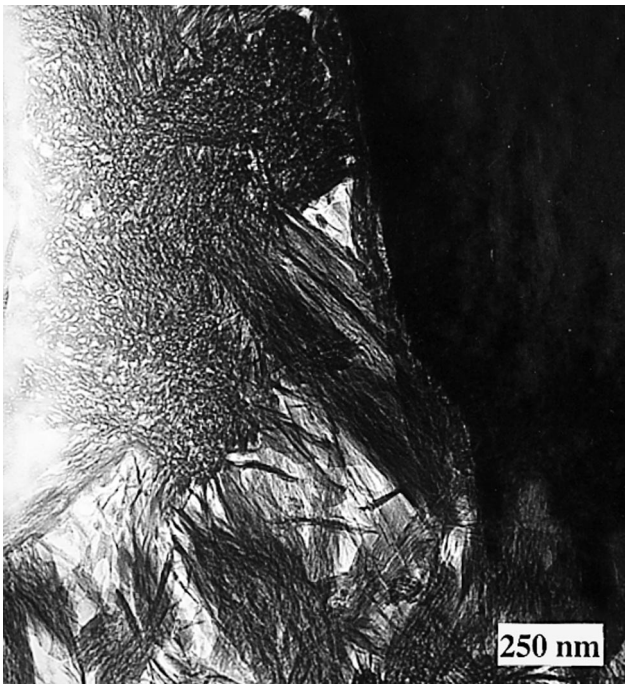

Fig. 3. Transmission electron micrograph showing a region in a mature C_3S paste which contains part of a crystal of CH and examples of Ip C–S–H and 'fine-fibrillar' Op C–S–H.

C–S–H – which are $\lesssim$10 nm; the boundary between interlayer space in the C–S–H and gel pores is ill-defined. Fig. 3 shows part of a large crystal of CH (right) and examples of Ip C–S–H and fine-fibrillar Op C–S–H (bottom), as observed in the TEM.

3.1.1.1. Nanostructure of C–S–H present in hardened C_3S and β-C_2S pastes. Although the average Ca/Si ratio remains essentially constant with degree of hydration, the nanostructure of the C–S–H present in hardened C_3S and β-C_2S pastes changes as hydration proceeds: trimethylsilylation (TMS) [9] and solid-state NMR studies [10,11] have established that C–S–H in young pastes consists mainly of dimeric silicate chains; as hydration proceeds some of the dimers are linked by monomers to form pentamers [12,13], and then possibly dimers and pentamers are linked by monomers to form octamers [12], thus giving a $2, 5, 8, \ldots, (3n-1)$ chain length sequence, where $n = 1, 2, 3$, etc. Some NMR data are included on Fig. 2 (bottom) [2,11,14]. In both C_3S and β-C_2S systems the C–S–H is initially dimeric with only a gradual increase in average silicate chain length ($\overline{CL}$) with hydration time: after 12 months hydration the $\overline{CL}$ for C–S–H from β-C_2S is about 2.7 and from C_3S is 3.3. Even after 26 yr the $\overline{CL}$ for C–S–H from C_3S is less than 5.

An example of a ^{29}Si NMR spectrum is shown in Fig. 4. This particular spectrum was from a ^{1}H–^{29}Si

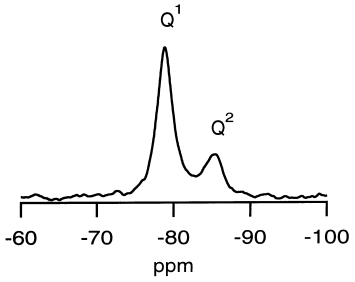

Fig. 4. ^{1}H–^{29}Si CP NMR spectrum of a β-C_2S paste hydrated for 1 month at 25°C; W/C = 0.4.

cross-polarization experiment in which only the hydrate phase is probed. The spectrum is from a β-C_2S paste hydrated for 1 month. The peaks at −78.9 and −85.3 ppm are due respectively to Q^1 and Q^2 species present in the C–S–H gel. This terminology is explained in Fig. 5, which shows schematic representations of pentameric silicate chains. Analysis in the TEM gave a mean Ca/Si ratio for the C–S–H of 1.71 ± 0.10 (26 analyses), and the single-pulse NMR spectrum gave an average silicate chain length of 2.6, which is in agreement with the data of Rodger which are reproduced on Fig. 2 [2].

Whilst any model for the structure of C–S–H phases must allow for a changing silicate anion structure with constant average Ca/Si ratio, it must also account for the marked variation in Ca/Si at the sub-micron scale [3]. Taylor [15] proposed a model for the structure of C–S–H based on finite silicate units derived from the 'dreierkette' structures of 1.4 nm tobermorite and jennite by the omission of some or all of the bridging tetrahedra; omission of all the bridging tetrahedra gives completely dimeric C–S–H. Fig. 5(a) shows a schematic representation of a pentameric silicate chain of the type present in Taylor's model. The O atoms at the bottom of the figure are also part of the central CaO_2 layer. Other workers have considered C–S–H to consist of tobermorite-based units in 'solid-solution' with CH [16–20] Richardson and Groves [21] proposed a general model which can be interpreted in terms of either of these approaches; the model may be represented as formula (1),

$$\left\{Ca_{2n}H_wSi_{(3n-1)}O_{(9n-2)}\right\}\cdot(OH)_{w+n(y-2)}\cdot Ca_{n.y/2}\cdot mH_2O, \tag{1}$$

where if $0\leqslant y\leqslant 2$ then $n(2-y)\leqslant w\leqslant 2n$, if $2\leqslant y\leqslant 4$ then $0\leqslant w\leqslant 2n$, and if $4\leqslant y\leqslant 6$ then $0\leqslant w\leqslant n(6-y)$. The model is based on a tobermorite-like core (that part of formula (1) contained within the braces) and consists of a highly disordered layer structure comprising finite silicate chains of average length $3n-1$. In immature cement pastes dimer is the most abundant silicate species ($n=1$). These are linked during polymerization by bridging tetrahedra to form pentamer ($n=2$) and higher polymers. The $2n$ Ca^{2+} ions within the braces are always

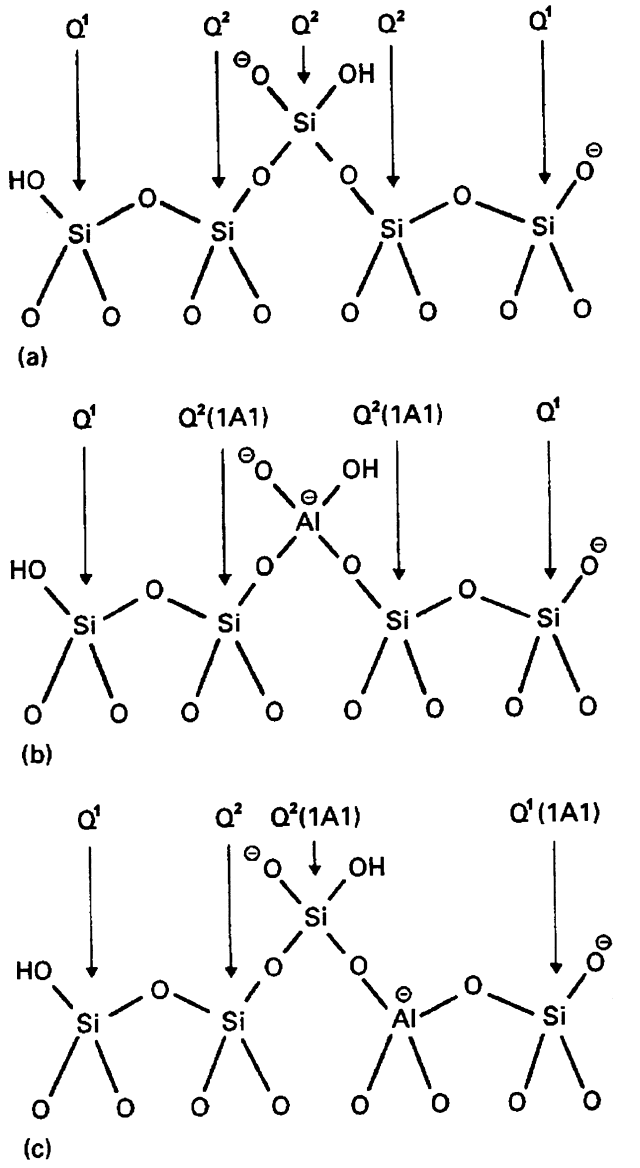

Fig. 5. (a) Schematic representation of a pentameric silicate chain of the type present in dreierkette-based models for the structure of C–S–H. Q^1 and Q^2 units are identified; the middle Q^2 unit is the 'bridging' tetrahedron; (b) The same as (a), but with Al^{3+} substituted for Si^{4+} in the bridging tetrahedron; (c) The same as (a), but with Al^{3+} substituted for Si^{4+} in a non-bridging tetrahedron. *Note*: ^{29}Si MAS NMR can provide quantitative information on the fractions of silicon present in different tetrahedral environments, Q^n ($0\leqslant n\leqslant 4$), where Q is a silicate tetrahedron and n is the number of oxygens which bridge to adjacent tetrahedra. Increased polymerization of the Q^n building units causes characteristic up-field chemical shifts. In alumino-silicates the shifts are further influenced by the replacement of Si by Al. There are 15 possible $Q^n(m\mathrm{Al})$ structural units where Q is a silicate tetrahedron connected via oxygen bridges to mAl and $n-m$ other Si atoms, with $n=0$ to 4 and $m=0$ to n. The following equations can be used to calculate the average chain length ($\overline{CL}$) and Al/Si ratio of Al-substituted C–S–H phases using the peak areas derived from deconvolution of single-pulse ^{29}Si NMR spectra:

$$\overline{CL}=\frac{2}{\left(\frac{Q^1}{Q^1+Q^2(0Al)+(3/2)Q^2(1Al)}\right)},\qquad Al/Si=\frac{(1/2)Q^2(1Al)}{Q^1+Q^2(0Al)+Q^2(1Al)}.$$

main layer Ca^{2+} ions, while there are always $n-(w/2)$ interlayer Ca^{2+} ions required for charge balance. The position of the remainder of the $(n\cdot y)/2$ Ca^{2+} ions outside of the braces depends on the structural viewpoint adopted. From the tobermorite/CH viewpoint they occur in layers of CH sandwiched between silicate layers of tobermorite-like structure while from the jennite/tobermorite viewpoint they form part of the main layer of jennite-based structural units (as ≡Si–O–Ca–OH). The structural units – and thus the parameters in the formula – may vary from one region of the C–S–H to another, thus accounting for the local variations in composition observed by TEM. For a given Ca/Si ratio and average chain length, the amount of hydroxyl water is defined by the variable w. In Taylor's model there is one silanol group per three tetrahedra which is given by $w=n$ in formula (1), and this is probably the most reasonable assumption for most portland cement-based systems. However, the compositions and average chain lengths of some C–S–H gels put them outside this assumption and so the extra flexibility in the possible degree of protonation inherent in formula (1) is necessary. An increase in w above its minimum value corresponds to increasing the number of ≡Si–OH and –Ca–OH bonds at the expense of ≡Si–O–Ca–O–Si≡. The Ca/Si ratio is given by

$$\mathrm{Ca/Si} = \frac{(4+y)n}{2(3n-1)}. \tag{2}$$

If we consider the general model from Taylor's viewpoint, as a mixture of structural units based on jennite and tobermorite with one silanol group per three tetrahedra (protonation level $w/n=1$), then for dimeric C–S–H ($n=1$) with minimum y ($y=1$) we get,

$$[\mathrm{Ca_2HSi_2O_7}]\cdot\frac{1}{2}\mathrm{Ca}\cdot m\mathrm{H_2O}$$

i.e. Taylors tobermorite-based dimer, $\mathrm{Ca/Si}=1.25$,

and with maximum y ($y=5$) we get,

$$\left[\mathrm{Ca_4HSi_2O_7(OH)_4}\right]\cdot\frac{1}{2}\mathrm{Ca}\cdot m\mathrm{H_2O}$$

i.e. Taylors jennite-based dimer, $\mathrm{Ca/Si}=2.25$.

Thus, we could envisage that the purely dimeric C–S–H present in young pastes with an average Ca/Si of 1.75 would consist of an equal mixture of tobermorite- and jennite-based units with Ca/Si of 1.25 and 2.25, respectively; this could account for the observed bimodal distribution of Ca/Si. Since Taylor's jennite-based pentameric structural unit has $\mathrm{Ca/Si}=1.8$, polymerization of the silicate chains with age would account for the observed change to a unimodal distribution [3]. If we consider the model from the tobermorite/CH viewpoint it is better represented by formula (3),

$$\mathrm{Ca}_X\mathrm{H}_{(6n-2X)}\mathrm{Si}_{(3n-1)}\mathrm{O}_{(9n-2)}\cdot z\mathrm{Ca(OH)_2}\cdot m\mathrm{H_2O}, \tag{3}$$

where, $X=\frac{1}{2}(6n-w)$; $z=\frac{1}{2}(w+n(y-2))$. For dimer (i.e. $n=1$), formula (3) reduces to:

$$\mathrm{Ca}_X\mathrm{H}_{(6-2X)}\mathrm{Si_2O_7}\cdot z\mathrm{Ca(OH)_2}\cdot m\mathrm{H_2O}. \tag{4}$$

This is the same formula as used previously by Glasser et al. [22] to describe the C–S–H predominant in young ordinary portland cement pastes.

The actual degree of protonation of the silicate chains in a C–S–H and the nature of the structural units (jennite/tobermorite or tobermorite/CH) probably depend on the conditions under which the C–S–H is formed. Many data seem to support the jennite/tobermorite structural viewpoint: for example, the observed bimodal distribution of Ca/Si of C–S–H in young portland cement pastes discussed above. Other data are consistent with treating high Ca/Si ratio C–S–H phases as a low Ca/Si C–S–H—CH 'solid-solution'. Stade and Wieker [23], for example, found that CH could be leached easily from high Ca/Si ratio C–S–H gels giving a residue with Ca/Si ≈1.25 but they could remove little from gels with low initial ratio, indicating a limiting value of extractable calcium. A limiting Ca/Si ratio is also found in the initial carbonation of C–S–H: Groves et al. [24] reported that a hardened C_3S paste which had been carbonated for 2 months in air (at 72.6% relative humidity) contained a relatively homogeneous C–S–H which ^{29}Si NMR showed to have an average silicate chain length of 4.5; silica gel had not yet formed. Eq. (2) predicts that a C–S–H with an average silicate chain length of 4.5 which was composed entirely of tobermorite-based structural units (i.e. $y=1$) would have a Ca/Si of 1.02. This was in excellent agreement with the mean Ca/Si determined directly in the TEM of 1.02 ± 0.12 (24 analyses). It was considered plausible that the Ca in excess of that required for charge-balancing the silicate chains with Ca^{2+} ions (i.e. the $z\mathrm{Ca(OH)_2}$ in formula (3)) should be the first Ca to be withdrawn from the C–S–H on reaction with CO_2, but it was not obvious why from the jennite/tobermorite viewpoint those Ca should be reactive since in that case they form an integral part of the main layer [21].

3.1.2. Portland cement pastes

The microstructure of a hardened ordinary portland cement paste contains, in addition to C–S–H and CH, two other major hydration products, produced from reactions involving the aluminate, alumino-ferrite, and calcium sulfate: AFt and AFm. AFt (Al_2O_3–Fe_2O_3-tri) phases have the general constitutional formula $[\mathrm{Ca_3(Al,Fe)(OH)_6\cdot 12H_2O}]_2\cdot X_3\cdot x\mathrm{H_2O}$ where x is $\leqslant 2$ and X generally denotes one formula unit of a doubly charged anion [25]. TEM analyses [3] of AFt relicts present in ordinary portland cement pastes gave the

ratios $(Al + Fe)/Ca = 1/3$ and $S/Ca = 1/2$ confirming that in ordinary portland cements X is SO_4^{2-}. AFm (Al_2O_3–Fe_2O_3-mono) phases have the general formula $[Ca_2(Al,Fe)(OH)_6] \cdot X \cdot xH_2O$ where X denotes one formula unit of singly charged anion, or a half a formula unit of a doubly charged anion [25]. In ordinary portland cements X is typically OH^- and SO_4^{2-}.

The identity and spatial distribution of hydrate phases present in a hardened cement paste can be studied readily by quantitative X-ray mapping in an electron microprobe. Fig. 6(a) shows a Ca/Si atom ratio X-ray map for a 50×50 μm^2 region in a hardened ordinary portland cement paste hydrated for 2 yr. The region is dominated by one partially hydrated grain. The white parts of the figure correspond to $Ca/Si > 2$, the shades of grey to $Ca/Si \leqslant 2$; the latter areas are thus mainly Ip C–S–H, or C–S–H admixed with small amounts of other phases. Scatter diagrams from the mapping data reveal the nature of the phase admixing at the level of the X-ray generation volume (≈1–2 μm^3). Fig. 7, a plot of Al/Ca against Si/Ca, shows that the region consists of unreacted alite (and, off the scale of the figure, some unreacted ferrite), C–S–H (mainly Ip but some Op), CH, AFm, and possibly some AFt; some points correspond to essentially pure phases whilst others correspond to mixtures of two or three phases.

The distribution of phases between Ip and Op is well-illustrated by a series of elemental ratio plots for a single line from the map, Fig. 8. The first few analyses (0–4 μm) are of Op. The next ~33 analyses correspond to the partially reacted alite grain; Ip–alite–Ip. Some of these analyses (e.g. 10–15) have very low S/Ca, whilst others have higher values (e.g. 6–8). The latter points, which also have higher Al/Ca ratios, correspond to admixture of Ip C–S–H with very small particles of AFm or AFt. Such sub-micron scale phase mixtures are readily observed by TEM; Fig. 9 shows Ip C–S–H and relicts of AFt crystals (AFt is very unstable under the electron beam). As in C_3S pastes, Ip C–S–H has a compact, fine-scale and homogeneous morphology, with pores $\lesssim$10 nm. Mg is never detected in TEM analyses of Op C–S–H. Since Mg remains in the Ip it can be used as a chemical marker for that region; the Mg map in Fig. 6(b) clearly reveals the shape of the partially reacted cement grain. TEM analyses reveal that Mg is present in Mg, Al-rich laths, which are intimately mixed with Ip C–S–H, Fig. 10. AFm particles present in the Ip have a similar appearance in the TEM and, as both phases are poorly crystalline and electron-beam sensitive, they are only differentiated from one another by X-ray microanalysis. CH is also observed in the Ip region; Fig. 11 shows an example of a large crystal. The inner product region thus consists of C–S–H with small amounts of all of the major phases (i.e. AFt, AFm, CH) and some minor phases; a Mg, Al-rich phase (hydrotalcite-like), and an Fe-rich phase [26] (a poorly crystalline hydrogarnet precursor). The bonding between Ip and Op C–S–H is generally excellent, with an often poorly defined interface [3].

Points 38–50 on Fig. 8 correspond to outer product. The Op region contains four major phases; C–S–H, CH, AFm and AFt. Of these, the C–S–H and CH are by far the most abundant. Calcium hydroxide typically occurs as massive crystals, often many micrometres in length.

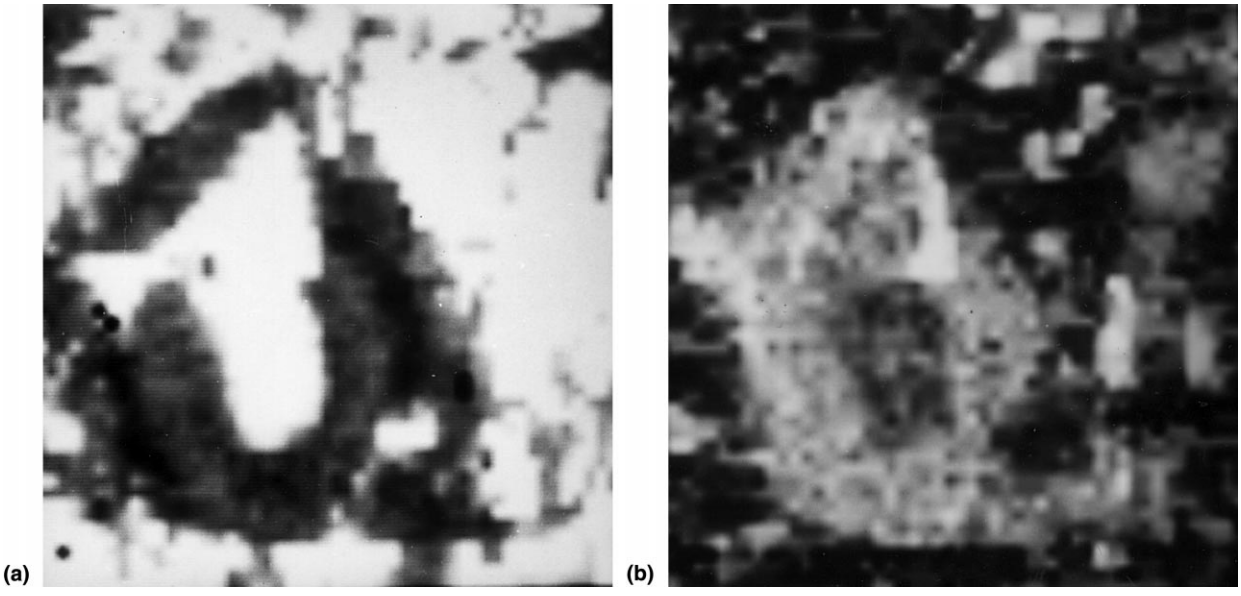

Fig. 6. (a) Ca/Si atom ratio map of an area (50×50 μm^2; 1 μm increments) in a 100% ordinary portland cement paste hydrated for 2 yr at 20°C, W/C = 0.4. (b) Mg atom map for the area in Fig. 6(a).

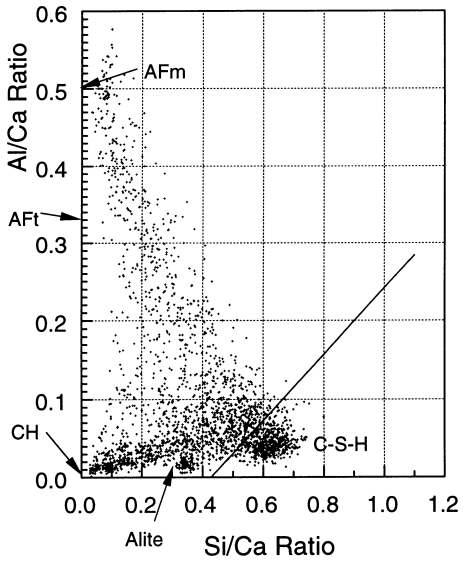

Fig. 7. Al/Ca against Si/Ca atom ratio plot for the EMPA mapping data of the area in Fig. 6.

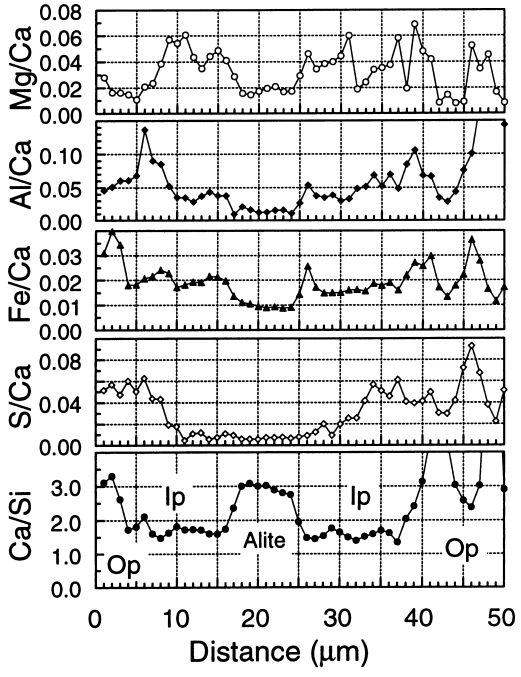

Fig. 8. Elemental ratio plots for one of the lines from the X-ray maps of the area in Fig. 6.

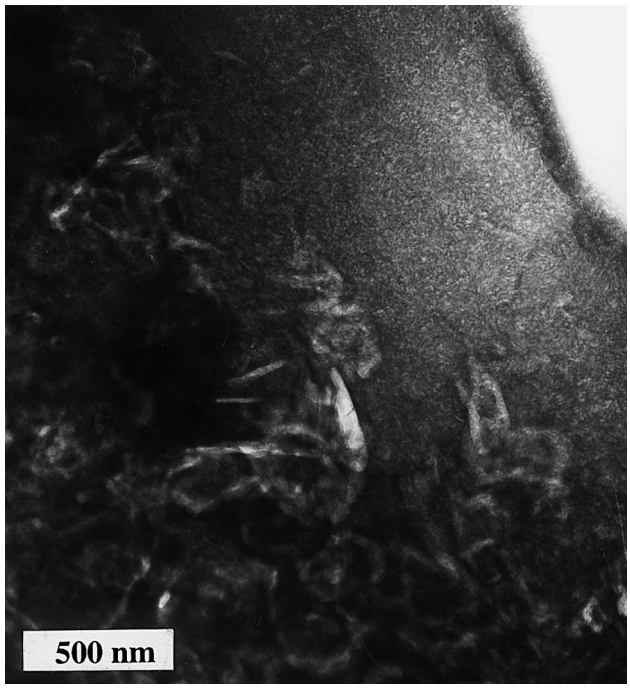

Fig. 9. Transmission electron micrograph showing AFt relicts in an inner product region in a mature ordinary portland cement paste.

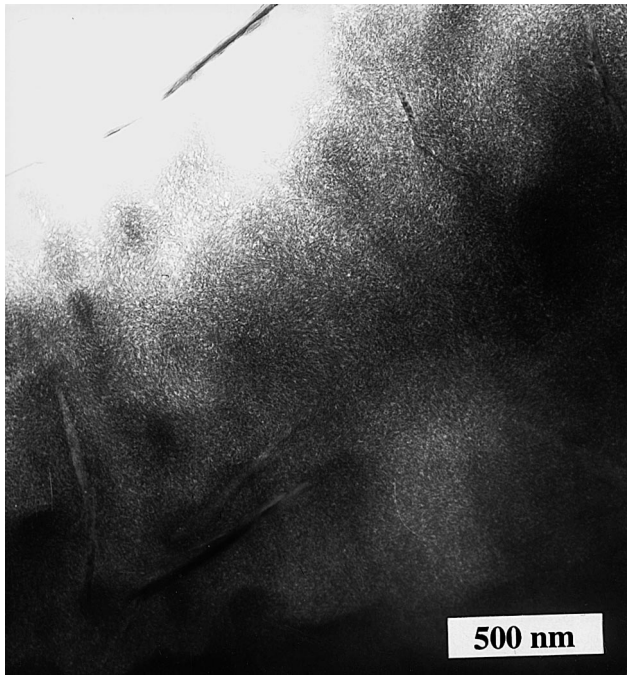

Fig. 10. Transmission electron micrograph showing Mg, Al-rich laths in a large inner product region in a mature ordinary portland cement paste.

Bonding with Op C–S–H is generally good. AFm is present in mature pastes as large irregular plates similar to those of CH. AFt occurs as thin hexagonal prism needles of up to 10 μm in length. The morphology of the C–S–H in hardened ordinary portland cement pastes is very similar to that in C_3S pastes: where it forms in large pore spaces, it exhibits a 'coarse fibrillar' morphology; in smaller spaces, it retains a directional aspect but forms in a more space-efficient manner ('fine fibrillar'). The latter is illustrated in Fig. 12, a TEM micrograph of a

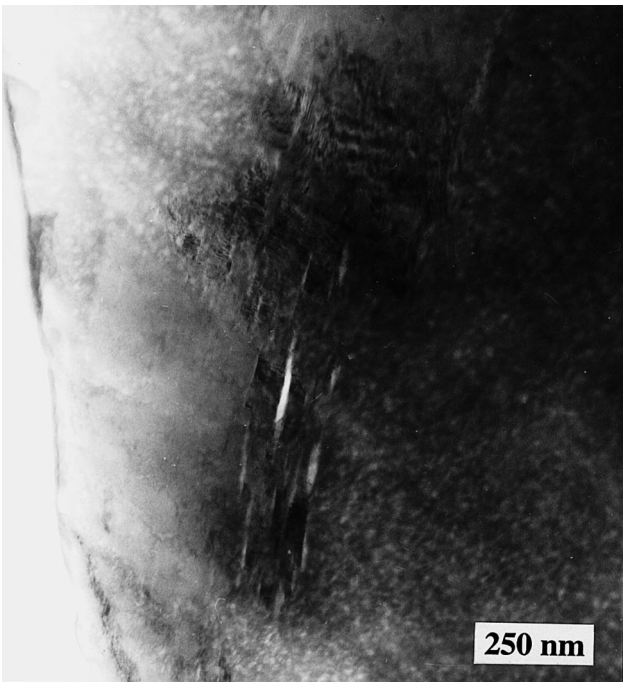

Fig. 11. Transmission electron micrograph showing a CH crystal embedded in inner product C–S–H.

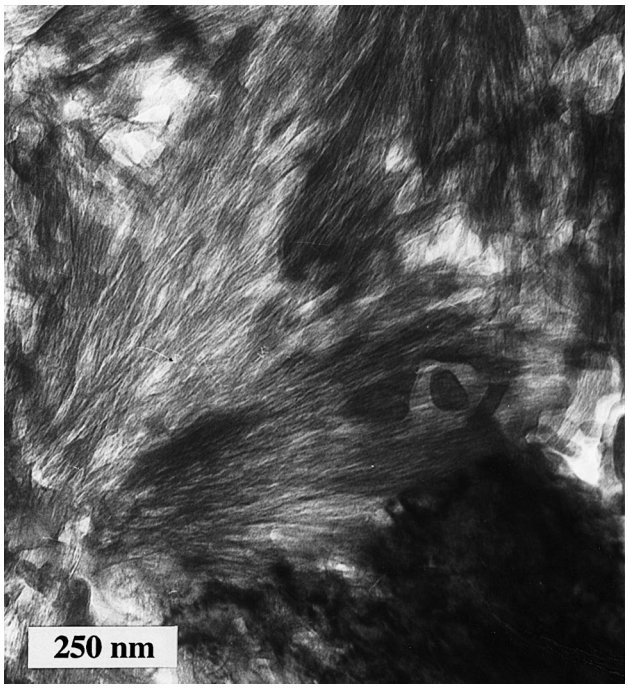

Fig. 12. Transmission electron micrograph showing a region in a mature ordinary portland cement paste which contains 'fine fibrillar' C–S–H, CH (bottom right), and a relict of AFt (just above the CH).

region which also contains CH (bottom right), and a relict of AFt (just above the CH).

3.1.2.1. Nanostructure of the C–S–H present in ordinary portland cement pastes. The C–S–H present in hardened ordinary portland cement pastes is compositionally similar to that present in C_3S and β-C_2S pastes with the difference that a small amount of Al is detected by microanalysis in the TEM; this is discussed in the section on slag–cement blends. The average Ca/Si ratio of both Ip and Op C–S–H is always 1.7–1.8 [3]. The silicate anion structure of the C–S–H is similar to that in C_3S and β-C_2S pastes; Fig. 13 shows a ^{1}H–^{29}Si CP NMR spectrum of a white portland cement paste hydrated for 5 months. The peaks at −78.9 and −85.0 ppm are due respectively to Q^1 and Q^2 species present in the C–S–H gel. Again, as in C_3S and β-C_2S pastes, whilst the average Ca/Si ratio of the C–S–H remains essentially constant as hydration proceeds [3], Fig. 2 (top; +), its average silicate chain length increases [2], Fig. 2 (bottom; +). As noted earlier, although the average Ca/Si ratio is always 1.7–1.8, there is significant variation at the micro- and nano-scales: a bimodal distribution in young pastes becomes unimodal as the paste matures [3].

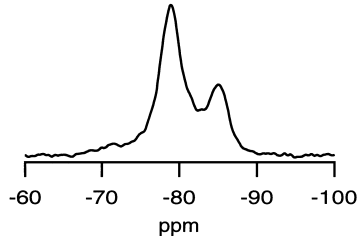

Fig. 13. ^{1}H–^{29}Si CP NMR spectrum of a white portland cement paste hydrated for 5 months at 25°C; W/C = 0.4.

3.1.3. Cements incorporating silica fume

Hardened pastes of cement–silica blends have distinct microstructures: they are denser due to the filling of spaces between cement grains by the fine silica particles, CH is consumed rapidly by pozzolanic reaction (although the C_3S or alite reactions are accelerated [14]), and the Ca/Si ratio of the C–S–H is reduced significantly. TEM imaging has shown that the morphology of Ip C–S–H from C_3S or alite grains is dependent on the silica content: in pastes containing 20% finely divided silica the Ip had the usual fine-texture [14], but in cement–silica fume pastes containing >50% silica fume, it had a foil-like morphology which was similar to that of the Op C–S–H; the Op region consisted of silica particles embedded in C–S–H with foil-like morphology [27].

3.1.3.1. Nanostructure of the C–S–H present in cements incorporating silica fume. Fig. 14 incorporates Dobson et al.'s [14] ^{29}Si NMR data for pastes of C_3S-20% finely divided silica (25°C; W/S = 0.5) (•--•), and Rodger et al.'s [11] data for pastes of neat C_3S for comparison

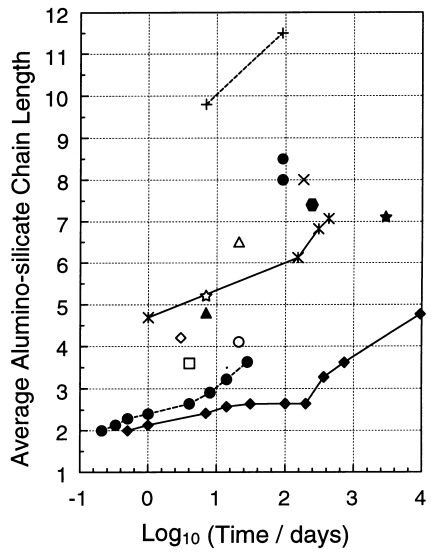

Fig. 14. Average alumino-silicate chain length against hydration time for C_3S–silica (•) (see text), and various slag-containing systems. The symbols for the latter are given in the key to Fig. 15(c).

(◆); the average silicate chain length of the C–S–H present in both systems increases with age, but it is significantly greater in the silica-containing system. Longer chain lengths are developed in systems with higher replacement; the data for the two points at greater chain length (same symbol, ●, but unconnected) are for C–S–H formed in a C_3S-silica system with overall Ca/Si of 1.0 hydrated for 3 months at 40°C (W/S = 0.7) [28], and in a ordinary portland cement–silica fume paste with >50% silica hydrated for 3 months at 40°C (W/S = 0.7) [27]. The C–S–H in the C_3S-silica system had $\overline{CL}$ of 8 and Ca/Si = 1; on the models for the structure of C–S–H this would be composed mainly of tobermorite-based structural units with either a small proportion of jennite-based units or CH in 'solid-solution'. The C–S–H present in the ordinary portland cement–silica fume paste had a mean Ca/Si ≈0.7–0.8 and $\overline{CL}$ of 8.5; this would be composed entirely of tobermorite-based units, but with a level of protonation greater than allowed in Taylor's model.

3.1.4. Portland cement–slag blends and alkali hydroxide-activated slag cements

The outer hydration products present in mature portland cement-slag blends are similar to those in neat portland cement; C–S–H, CH, and AFm. As the proportion of slag is increased the composition and morphology of the C–S–H change and the contents of CH and AFm decrease, with the AFm phase also incorporating more S [29]. There is no CH or AFm present in neat water-activated slag systems, although AFm is present when the slag is activated by concentrated alkali-hydroxide solution [30]. Microanalysis in the TEM of the Op C–S–H present in a range of slag-containing hardened cement pastes has shown that as the proportion of slag increases the Al/Ca ratio increases linearly with increasing Si/Ca ratio, Fig. 15(a). This figure incorporates data of Richardson and Groves' for a range of ordinary portland cement–slag blends [29–31] (SC slag in Table 1; hydrated at 20°C for 14 months (W/S = 0.4)(●)), some slag/KOH pastes made with the same slag (■), and a synthetic slag/KOH paste (▲). The regression line ($r^2 = 0.98$) represents,

$$\mathrm{Si/Ca} = 0.4277 + (2.366 \times \mathrm{Al/Ca}). \quad (5)$$

As the Al/Ca and Si/Ca ratios increase, the contents of CH (+) and AFm (×) decrease, Fig. 15(b). The compositions of the Op C–S–H gels present in slag cement blends using a white cement and a different slag (VL slag in Table 1) (○, △) are similar to those in the ordinary portland cement/SC slag blends despite having different portland cements and different blast-furnace slags, Fig. 15(c); the compositional trend line on this figure is derived from the data in Fig. 15(a), i.e. Eq. (5). This line is also reproduced on Figs. 16(a)–(d) which are Al/Ca against Si/Ca scatter diagrams for EMPA mapping data from regions in four cement–slag blends containing 10%, 50%, 83%, and 90% of slag. Such diagrams reveal the nature of the phase admixing at the level of the X-ray generation volume (≈1–2 μm^3); some points correspond to essentially pure phases whilst others correspond to mixtures of two or three phases. The region in the 10% slag paste consists of C–S–H, CH, AFm, a Mg, Al-rich phase (hydrotalcite-like, HT), unreacted slag (and, off the scale of the figure, some unreacted ferrite). As the proportion of slag in the blend increases, the amount of CH and AFm reduce, and the Al/Ca and Si/Ca ratios of the C–S–H increase; there is excellent agreement between these data and the compositional trend line derived from TEM analyses of Op C–S–H free of admixture with other phases. The C–S–H in the KOH-activated slag cement pastes mostly fall on the same compositional trend line, Fig. 15(c), suggesting an almost universal compositional relationship for the C–S–H phases present in slag-containing hardened cement systems. It is notable that the approximate composition of the C–S–H present in a portland cement – 28% fly ash blend [32] falls close to the line (point ◆ on Fig. 15(c)); this suggests that Eq. (5) may be valid for C–S–H phases in all cementitious calcium alumino-silicate systems.

As the fraction of slag in cement–slag blends increases, a foil-like morphology gradually replaces the more linear morphology. This is illustrated in Figs. 17–20, which are TEM micrographs of Op C–S–H present in a cement–slag blend containing 50% slag, and in water-, CH- and KOH-activated slag pastes. The foil-like morphology appears to be more effective in filling

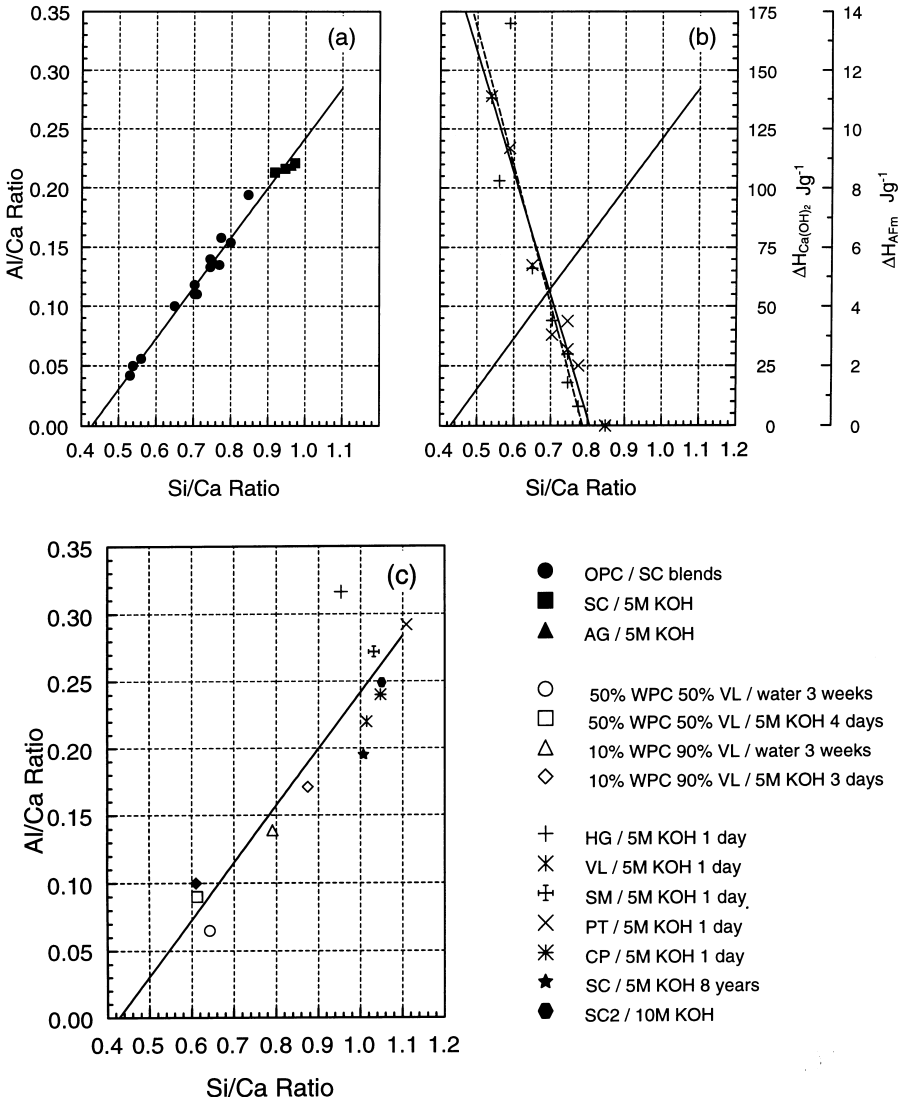

Fig. 15. (a) Al/Ca against Si/Ca plot of TEM analyses of Op C–S–H in a range of slag-containing hardened cement pastes. Each point corresponds to a mean value of 20–50 analyses of Op C–S–H free of admixture with other phases. The equation for the regression line (Eq. (5)) and the key is given on the text; (b) Plots of AFm (×) and CH (+) against Si/Ca ratio of the Op C–S–H present in the cement–slag blends; (c) Al/Ca against Si/Ca plot of TEM analyses of Op C–S–H in water and KOH-activated white portland cement–VL slag blends, and in KOH-activated slags with a range of compositions; see Table 1 for details. Each point corresponds to a mean value of 20–50 analyses of Op C–S–H free of admixture with other phases. The line is derived from the data in (a), i.e. Eq. (5).

space without leaving large interconnected capillary pores. The average Ca/Si ratios of Op C–S–H or Ip C–S–H derived from alite or slag grains do not differ significantly from one another, nor is there any significant change in average Ca/Si with the age of the paste [29]. In portland cement–slag blends, inner product C–S–H may be derived from alite, belite, or slag grains. In the case of alite and belite, the C–S–H generally displays the fine homogenous texture typical of the Ip C–S–H in neat portland cement pastes. Slag-grain Ip most commonly has a similar fine homogeneous morphology, Fig. 21, but it is distinctive in having a high content of Mg and Al. Laths and platelets are often observed which are particularly rich in Mg, Al, and Ti. These sometimes take the form of poorly developed laths, randomly distributed in Ip which has a high proportion of C–S–H, Fig. 22, or sometimes as well-developed platelets oriented towards the Ip/Op boundary, Fig. 23, and often occupying most of the Ip, as in Fig. 24. The various stages of development of this Mg, Al-rich precipitate occur simultaneously within the same specimen. Since Mg does not migrate from the volume originally occupied by the slag grain, it becomes relatively more concentrated as reaction proceeds to form Ip, and therefore forms an excellent chemical marker for slag Ip in X-ray mapping; this is illustrated in Fig. 25, a

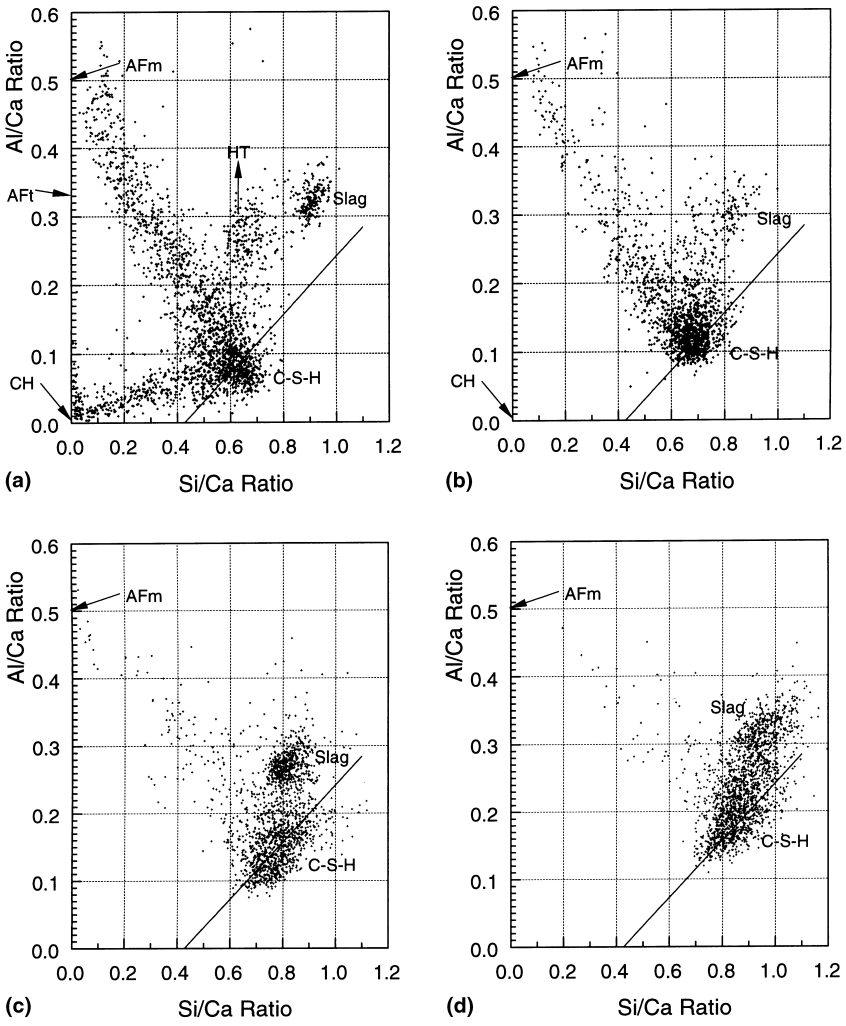

Fig. 16. (a) Al/Ca against Si/Ca atom ratio plot for the EMPA mapping data of an area (50×50 μm^2; 1 μm increments) in a 90% ordinary portland cement 10% slag paste hydrated for 14 months; (b) Al/Ca against Si/Ca atom ratio plot for the EMPA mapping data of an area (40×40 μm^2; 1 μm increments) in a 50% ordinary portland cement 50% slag paste hydrated for 14 months; (c) Al/Ca against Si/Ca atom ratio plot for the EMPA mapping data of an area (50×55 μm^2) in a 17% ordinary portland cement 83% slag paste hydrated for 14 months; (d) Al/Ca against Si/Ca atom ratio plot for the EMPA mapping data of an area (45×40 μm^2) in a 10% ordinary portland cement 90% slag paste hydrated for 14 months.

Mg atom map of a 40×40 μm^2 region in a 75% ordinary portland cement 25% SC slag blend hydrated for 14 months. The region contains one prominent partially reacted slag grain adjacent to a smaller fully reacted grain. Fig. 26 shows a series of elemental ratio plots for a single line from the map which includes both of these grains; analyses corresponding to Op, Ip and unreacted slag are indicated. Plots of Mg/Ca against Al/Ca from microanalysis in both EMPA and TEM show a linear relationship which can be described by the equation [29]:

$$\mathrm{Al/Ca} = a + b(\mathrm{Mg/Ca}). \quad (6)$$

This relationship is due to different levels of admixture within the analysed volume of the Mg, Al-rich phase, which has an Al/Mg ratio b, and a single phase C–S–H with Al/Ca ratio a. The Al/Ca ratio of the single-phase C–S–H present in slag- and alite/belite-grain Ip is similar to that of the Op C–S–H. Thus inner product can be viewed as a single-phase C–S–H which is compositionally equivalent to Op C–S–H, intermixed over a range of scales with varying amounts of a Mg, Al-rich hydroxide phase, and in low slag blends, also with small amounts of AFm; Ip is compositionally identical to Op C–S–H but with the addition of elements of brucite-based and AFm-type phases with the generalized formula,

$$\left[\mathrm{R}^{2+}_{1-k}\mathrm{R}^{3+}_{k}(\mathrm{OH})_2\right]^{k+} \cdot \mathrm{R}^{r-}_{k/r} \cdot j\mathrm{H_2O},$$

where typically for brucite-based phases $\mathrm{R}^{2+} = \mathrm{Mg}^{2+}$; $\mathrm{R}^{3+} = \mathrm{Al}^{3+}$ or Fe^{3+}; $\mathrm{R}^{r-} = \mathrm{OH}^-$, SO_4^{2-}, CO_3^{2-} and for AFm phases $\mathrm{R}^{2+} = \mathrm{Ca}$; $\mathrm{R}^{3+} = \mathrm{Al}^{3+}$ or Fe^{3+}; $R^{r-} = \mathrm{OH}^-$, SO_4^{2-}, CO_3^{2-}, or other common anions. For brucite-based phases (i.e. hydrotalcite-like) $\sim \frac{1}{5} \leqslant k \leqslant \frac{1}{3}$ [34,35] whereas for AFm phases k has a fixed value of $\frac{1}{3}$. In

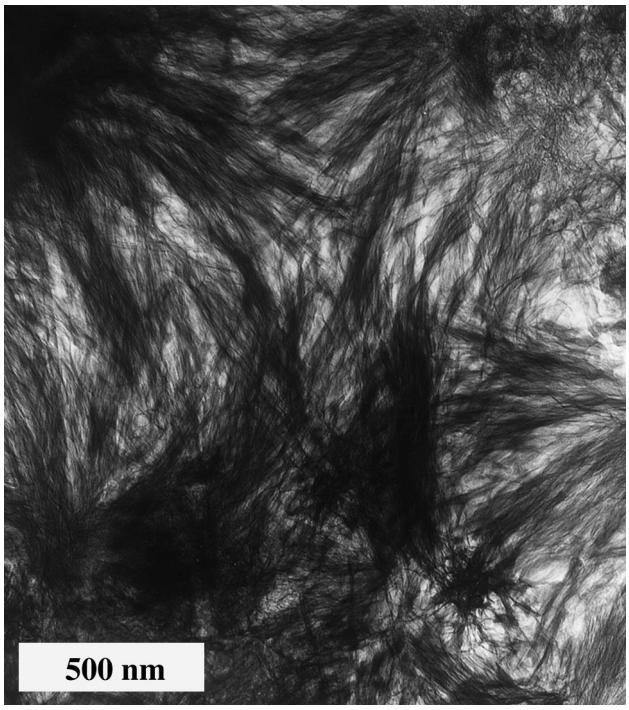

Fig. 17. Transmission electron micrograph showing 'fine fibrillar' Op C–S–H in a 50% ordinary portland cement 50% slag paste hydrated for 1 month.

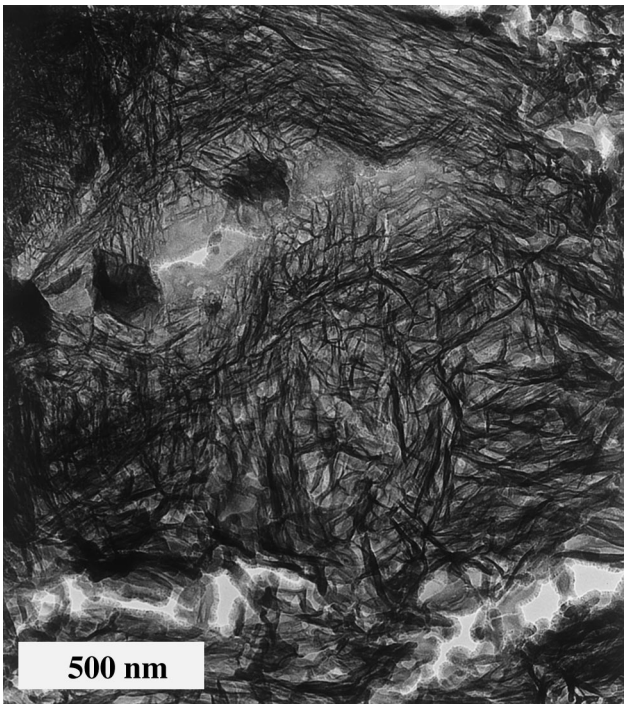

Fig. 19. Transmission electron micrograph showing foil-like Op C–S–H in a CH-slag paste hydrated for $3\frac{1}{2}$ yr.

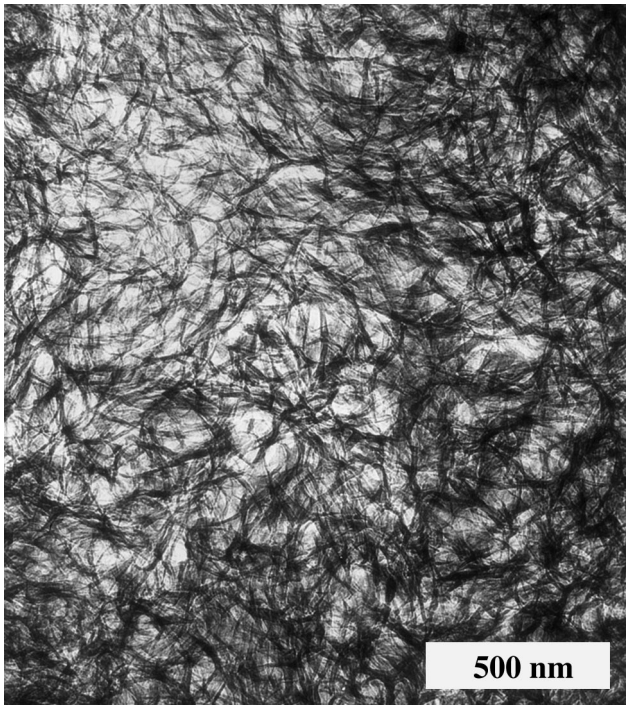

Fig. 18. Transmission electron micrograph showing foil-like Op C–S–H in a water-activated 100% slag paste hydrated for $3\frac{1}{2}$ yr.

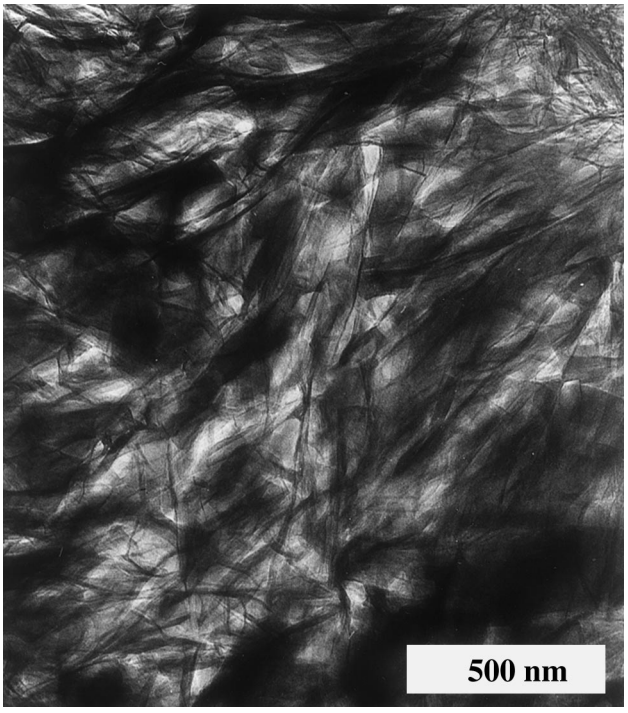

Fig. 20. Transmission electron micrograph showing foil-like Op C–S–H in a 5*M* KOH-activated 100% slag paste hydrated for 8 yr.

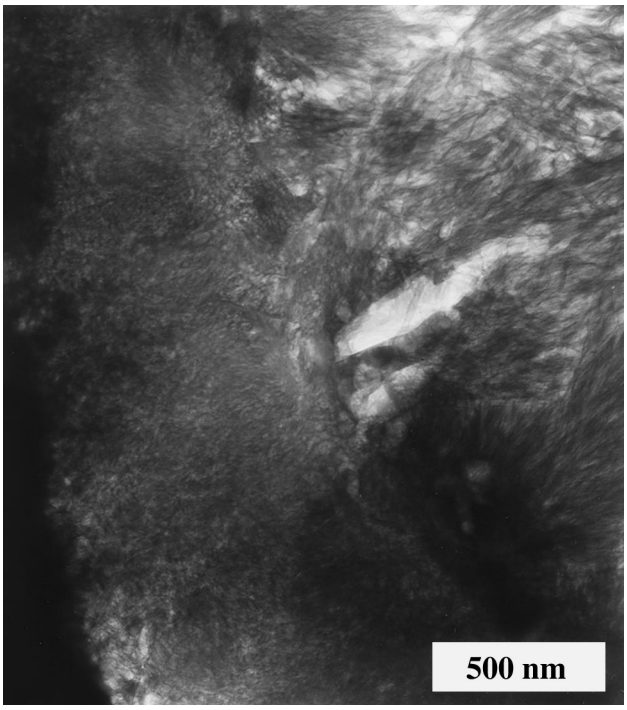

Fig. 21. Transmission electron micrograph showing fine-textured Ip and 'fine fibrillar' Op C–S–H in a 50% ordinary portland cement 50% slag paste hydrated for $2\frac{1}{2}$ yr.

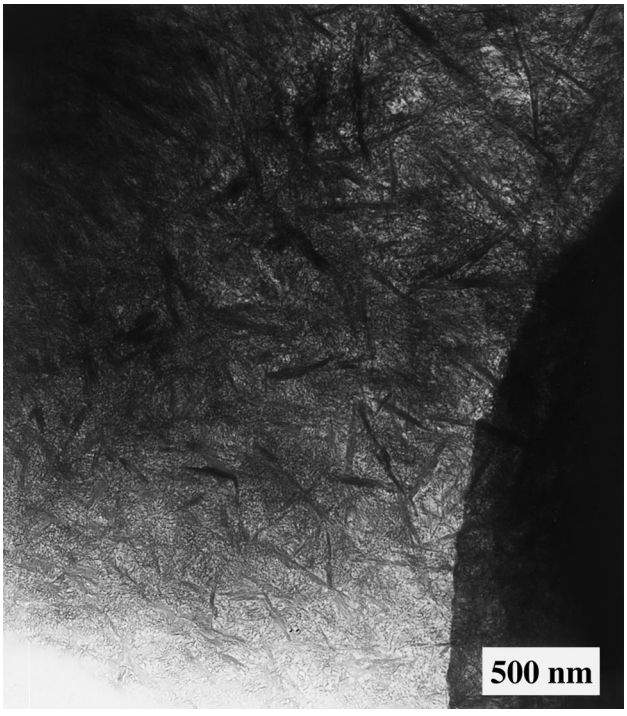

Fig. 22. Transmission electron micrograph showing Mg, Al-rich precipitates randomly distributed within a slag inner product region in a 33% ordinary portland cement 67% slag paste hydrated for 14 months.

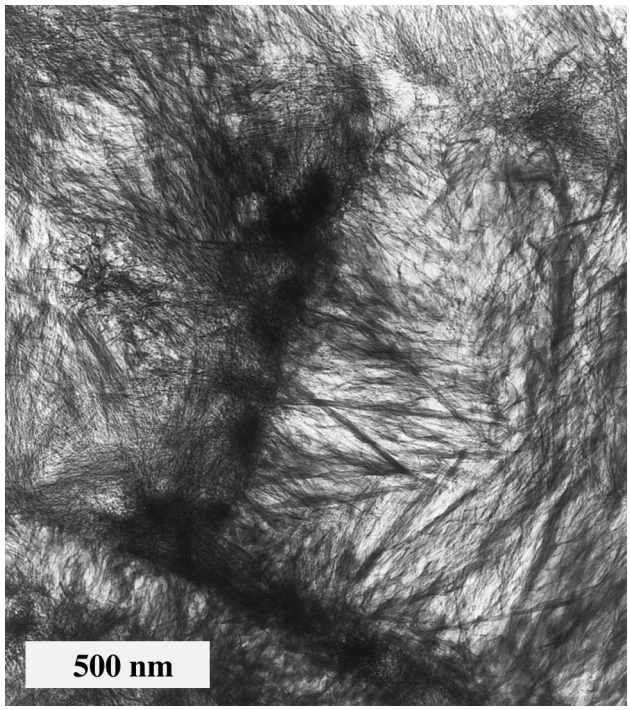

Fig. 23. Transmission electron micrograph showing a well-defined slag inner product region containing C–S–H and Mg, Al-rich precipitates which are oriented towards the Ip/Op interface in a 17% ordinary portland cement 83% slag paste hydrated for 14 months.

Fig. 24. Transmission electron micrograph showing a well-defined slag inner product region containing Mg, Al-rich precipitates which are oriented towards the Ip/Op interface in a 50% ordinary portland cement 50% slag paste hydrated for 1 month.

Fig. 25. Mg atom map of an area (40×40 μm^2; 1 μm increments) in a 25% ordinary portland cement 75% slag paste hydrated for 14 months.

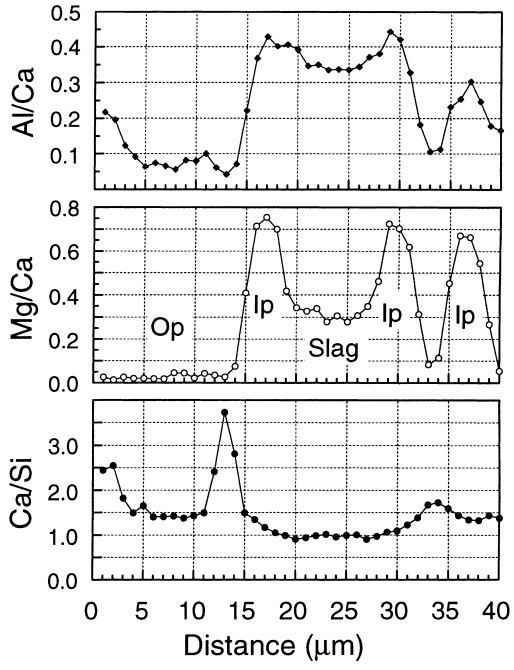

Fig. 26. Elemental ratio plots for one of the lines from the X-ray maps for the area in Fig. 25.

portland cement–slag blends b in Eq. (6) has an average value of 0.42 but with anomalously low and high values for the 0% and 100% slag pastes [29]; KOH-activation of six of the slags in Table 1 (SC, HG, VL, SM, PT, AG), gave an average value for b of 0.41 [33].

3.1.4.1. Nanostructure of the C–S–H present in slag cement pastes. The linear increase in Al/Ca with Si/Ca ratio of the C–S–H, shown in Fig. 15(a), suggests that there is a structural limitation on the incorporation of Al; Richardson and Groves [31] assumed that Al substitutes for Si solely at bridging sites in a 'dreierkette' chain structure. The experimental points on Figs. 15(a) and (c) therefore represent compositions of C–S–H phases of chain length increasing with increasing Si/Ca. The lowest Si/Ca ratio observed is only slightly greater than that of dimer (jennite-based dimer Si/Ca = 0.44) which, as it contains no bridging tetrahedra, contains no Si which can be substituted by Al. As the average chain length increases above that of the dimer, the inclusion of bridging tetrahedra rapidly increases the maximum possible degree of Al substitution. The general model modified to incorporate substituents can be represented as formula (7) [31],

$$\left\{Ca_{2n}H_w\left(Si_{1-a}R_a^{[4]}\right)_{(3n-1)}O_{(9n-2)}\right\}\cdot I^{c+}_{a/c(3n-1)} \cdot (OH)_{w+n(y-2)}\cdot Ca_{n.y/2}\cdot mH_2O, \quad (7)$$

where $R^{[4]}$ is a trivalent cation, mainly Al^{3+}, in tetrahedral co-ordination and I^{c+} is an interlayer ion, either a monovalent alkali cation or Ca^{2+}, charge-balancing the R^{3+} substitution for Si^{4+}. Al is assumed to only substitute for Si in the bridging tetrahedra of the dreierkette structure; since there are $n-1$ bridging sites,

$$0 \leqslant a \leqslant \frac{n-1}{3n-1}.$$

From the tobermorite/$Ca(OH)_2$ structural viewpoint the model is better represented by formula (8),

$$Ca_XH_{(6n-2X)}\left(Si_{1-a}R_a^{[4]}\right)_{(3n-1)}O_{(9n-2)}\cdot I^{c+}_{a/c(3n-1)} \cdot zCa(OH)_2\cdot mH_2O, \quad (8)$$

where, $X = \frac{1}{2}(6n-w)$; $z = \frac{1}{2}(w+n(y-2))$.

Initial support for the model was provided by Richardson and co-workers' determination of the location of Al in semi-crystalline substituted C–S–H phases [30,36,37] which were formed by the reaction of a slag (SC in Table 1) and a synthetic slag-glass (AG) with 5M KOH solution. The single-pulse ^{29}Si and ^{1}H–^{29}Si CP MAS NMR spectra gave conclusive evidence that Al substituted for Si solely in the central tetrahedron of pentameric linear chains (or in every third tetrahedron in longer chains), as illustrated in Fig. 5(b): since there were no Q^1(1Al) units on the ^{29}Si CP MAS NMR spectra Al could – assuming no chain terminating Al – only be substituted for Si in bridging tetrahedra; Q^1(1Al) units would be expected if Al substituted for Si at non-bridging Q^2 sites, as in Fig. 5(c). There could be no significant number of chain terminating Al as this would have produced higher Al/Si ratios derived from NMR than from analytical TEM which gives unambiguous compositions; in fact there was good agreement.

Excellent agreement has also been found for the C–S–H gels from KOH-activation of the slags detailed in Table 1, which have a wide range of glass composition [33]. High Al/Si of the slag-glass leads to high Al/Si of the C–S–H and to long $\overline{CL}$; the number of occupied bridging sites that are occupied by Al and not Si is high in all cases [33]. As with the C–S–H phases present in neat portland cement and in cement–slag blends the $\overline{CL}$ increases with age whilst the chemical composition remains essentially constant.

More recent work has provided data to support the model's applicability to C–S–H phases present in water-activated cement–slag blends [7]. Fig. 27(a) shows a single-pulse ^{29}Si NMR spectrum for anhydrous white portland cement; the sharp Q^0 peak at −71.3 ppm corresponds to the belite phase and is superposed on a broader peak due to alite. Figs. 27(b)–(d) show single-pulse ^{29}Si NMR spectra for white portland cement–slag blends with 0%, 50% and 90% slag activated with water ((b), (c), (d); hydrated for 4, 20 and 18 days). In Fig. 27(b), the neat portland cement paste, there are clearly two peaks at around −79 and −85 ppm, which correspond to Q^1 and Q^2 species present in the C–S–H. The spectra for the blends ((c) and (d)) appear to have three hydrate peaks, Q^1, Q^2(1Al), and Q^2, but they are not well-resolved and more information is needed to deconvolute them. Such information can be obtained by activating the white cement–slag blends with 5*M* KOH solution. The hydration products and microstructures of the KOH-activated and water-activated blends are very similar: with both activators the main outer products are C–S–H, CH and AFm, and Ip can be considered with both to be an intimate mixture of C–S–H and a Mg, Al hydroxide type phase. However, whilst the CH in the water-activated blends generally occurs as large plates and the C–S–H is nearly amorphous, in the KOH-activated pastes the CH is largely microcrystalline, being intimately mixed on a nanometre scale with layers of C–S–H [7], and the C–S–H is semi-crystalline which leads to narrower NMR linewidths and thus to improved resolution. Figs. 27(e)–(h) show single-pulse ^{29}Si NMR spectra for white portland cement–slag blends with 0%, 50%, 90%, and 100% slag activated with 5*M* KOH solution ((e), (f), (g), (h); hydrated for 4, 4, 3, and 1 days). Fig. 27(h) also includes results of the deconvolution of the spectrum. The hydrate peaks in these spectra are very clearly defined, and the results from their deconvolution have been used to aid in the deconvolution of the spectra from the water-activated pastes [7]; the peak areas allow calculation of the average Al/Si ratio of the C–S–H in the paste – i.e. in both the Op and Ip – and of the average alumino-silicate chain length ($\overline{CL}$), Fig. 5. The compositions derived from the deconvolution of the NMR spectra are in excellent agreement with those measured directly in the TEM [7,33]; the assumptions that there are no chain-terminating Al, and that Al only substitutes for Si at tetrahedral bridging sites, would seem therefore to be well-founded. The absence of Q^1(1Al) peaks on the ^{1}H–^{29}Si CP spectra also supports the view that the higher polymers are formed by the linking of dimeric silicate units by silicate or aluminate monomers; there can be no aluminate-containing dimers. The number of occupied bridging sites that are occupied by Al and not Si is 72 and 83% for the C–S–H gels in the KOH-activated 50% and 90% slag blends respectively; water-activation produces only 3/4 as much Al substitution as does KOH. The $\overline{CL}$ of the C–S–H present in these systems are much greater than in C_3S or ordinary portland cements, Fig. 14.

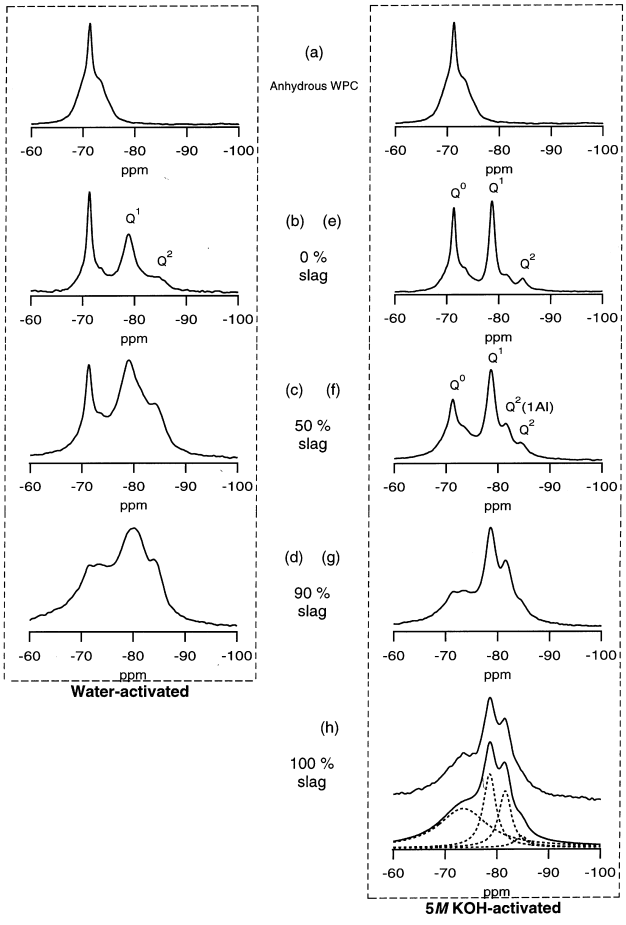

Fig. 27. Single-pulse ^{29}Si NMR spectra for anhydrous white portland cement (a), and blends with 0%, 50%, and 90% slag activated with water, (b), (c), (d) hydrated for 4, 20, and 18 days, and 5*M* KOH solution, (e), (f), (g) hydrated for 4, 4, and 3 days, and for KOH-activated slag (h) hydrated for 1 day.

4. Conclusions

The microstructure of hardened C_3S pastes serves as a useful reference for the more complex systems: for

ordinary portland cement and blends of portland cement with silica fume and ground granulated iron blast-furnace slag, and for alkali-hydroxide activated slag cements. The reference microstructure consists of unreacted material, and 'outer' (Op) and 'inner' (Ip) hydration products; outer products form in the originally water-filled spaces and inner products within the boundaries of the original C_3S grains. In hardened C_3S or portland cement pastes Op C–S–H has a fibrillar, directional morphology. The spaces between the fibrils constitute the capillary porosity, a three-dimensional interconnected pore network which is of major importance for durability. In portland cements blended with silica fume the average silicate chain length of the C–S–H phase increases with increasing Si/Ca ratio and its morphology changes from fibrillar to foil-like. In portland cements blended with slag the Si/Ca and Al/Ca ratios of the C–S–H increase as the proportion of the slag is increased, the alumino-silicate chains get on average longer, and its morphology changes from fibrillar to foil-like. All C–S–H phases in such systems, whatever their chemical composition or degree of structural order, have aluminium substituting for silicon only in the central tetrahedron of pentameric silicate chains (or in every third tetrahedron in longer chains). This gives considerable confidence in models for the structure of C–S–H based on broken dreierkette chains with Al substituting for Si at 'bridging' sites only; a general dreierkette-based model is applicable to the C–S–H phases present in all these systems. The change in C–S–H morphology from fibrillar to foil-like results in a less well-interconnected capillary pore structure. Provided that the mineral addition is well-reacted this would largely account for the lower permeabilities – and so enhanced durability – of such systems.

Acknowledgements

Thanks are due to the Engineering and Physical Sciences Research Council for funding under Grant Nos. GR/H64972 and GR/K52089, to Dr Geoff. Groves and Prof. Joe Cabrera for encouragement and support, and to Prof. Neville Boden (SOMS Centre, University of Leeds) and Prof. Chris Dobson FRS (Inorganic Chemistry Lab., University of Oxford) for provision of the NMR facilities.

References

[1] Groves GW, LeSueur PJ, Sinclair W. Transmission electron microscopy and microanalytical studies of ion-beam-thinned sections of tricalcium silicate paste. J Am Ceram Soc 1986;69:353–6.
[2] Rodger SA. D. Phil. thesis. University of Oxford, 1984.
[3] Richardson IG, Groves. The microstructure and microanalysis of hardened ordinary Portland cement pastes. J Mater Sci 1993;28:265–77.
[4] Rocha J, Klinowski J. Kaolinite as a convenient standard for setting the Hartmann–Hahn match for ^{29}Si CP MAS NMR of silicates. J Magn Reson 1990;90(3):567–8.
[5] WaveMetrics, Inc., Igor (1992) and Igor Pro (1996), Lake Oswego, Oregon, 97035, USA.
[6] Brough AR. D.Phil. thesis. University of Oxford, 1993.
[7] Richardson IG, Groves GW. The structure of the calcium silicate hydrate phases present in hardened pastes of white Portland cement/blast-furnace slag blends. J Mater Sci 1997;32:4793–802.
[8] Groves GW. TEM studies of cement hydration. Mat Res Soc Symp Proc 1987;85:3–12.
[9] Dent-Glasser LS, Lachowski EE, Mohan K, Taylor HFW. A multi-method study of C_3S hydration. Cem Concr Res 1978;8:733–40.
[10] Clayden NJ, Dobson CM, Groves GW, Rodger SA. The application of solid-state nuclear magnetic resonance spectroscopy techniques to the study of the hydration of tricalcium silicate. Proceedings of the eighth International Congress Chem. Cem. III 1986;51–6.
[11] Rodger SA, Groves GW, Clayden NJ, Dobson CM. Hydration of tricalcium silicate followed by ^{29}Si NMR with cross-polarization. J Am Ceram Soc 1988;71(2):91–6.
[12] Hirljac J, Wu Z-Q, Young JF. Silicate polymerization during the hydration of alite. Cem Concr Res 1983;13:877–86.
[13] Dent-Glasser LS, Lachowski EE, Qureshi MY, Calhoun HP, Embree DJ, Jamieson WD, Masson CR. Identification of some of the polysilicate components of trimethylsilylated cement paste. Cem Concr Res 1981;11:775–80.
[14] Dobson CM, Goberdhan GCD, Ramsay JDF, Rodger SA. ^{29}Si MAS NMR study of the hydration of tricalcium silicate in the presence of finely divided silica. J Mater Sci 1988;23:4108–14.
[15] Taylor HFW. Proposed structure for calcium silicate hydrate gel. J Am Ceram Soc 1986;69:464–7.
[16] Greenberg SA, Chang TN, Anderson E. J Phys Chem 1960;64:1151.
[17] Greenberg SA, Chang TN. J Phys Chem 1965;69:182.
[18] Fujii K, Kondo W. Estimation of thermochemical data for calcium silicate hydrate (C–S–H). J Am Ceram Soc 1983;66:C-220–1.
[19] Kantro DL, Brunauer S, Weise CH. Development of surface in the hydration of calcium silicates. II Extension of investigations to earlier and later stages of hydration. J Phys Chem 1962;66:1804.
[20] Birchall JD, Thomas NL. The mechanism of retardation of setting of OPC by sugars. Proc Brit Ceram Soc 1984;35:305–15.
[21] Richardson IG, Groves GW. Models for the composition and structure of calcium silicate hydrate (C–S–H) gel in hardened tricalcium silicate pastes. Cem Concr Res 1992;22:1001–10.
[22] Glasser FP, Lachowski EE, Macphee DE. Compositional model for calcium silicate hydrate (C–S–H) gels, their solubilities, and free energies of formation. J Am Ceram Soc 1987;70:481–5.
[23] Stade H, Wieker W. On the structure of ill-crystallized calcium hydrogen silicates, I. Formation and properties of an ill-crystallized calcium hydrogen disilicate phase. Z Anorg Allg Chem 1980;466:55–70 [in German].
[24] Groves GW, Rodway DI, Richardson IG. The carbonation of hardened cement pastes. Adv Cem Res 1990;3:117–25.
[25] Taylor HFW. Cement chemistry, 2nd ed. London: Thomas Telford, 1997.
[26] Rodger SA, Groves GW. Electron microscopy study of ordinary portland cement and ordinary portland cement-pulverized fuel ash blended pastes. J Am Ceram Soc 1989;72(6):1037–9.
[27] Groves GW, Rodger SA. The hydration of C_3S and ordinary portland cement with relatively large additions of microsilica. Adv Cem Res 1989;2(8):135–40.

[28] Brough AR, Dobson CM, Richardson IG, Groves GW. A study of the pozzolanic reaction by solid-state ^{29}Si nuclear magnetic resonance using selective isotopic enrichment. J Mater Sci 1995;30:1671–8.

[29] Richardson IG, Groves GW. The microstructure and microanalysis of hardened cement pastes involving ground granulated blast-furnace slag. J Mater Sci 1992;27:6204–12.

[30] Richardson IG, Brough AR, Groves GW, Dobson CM. The characterization of hardened alkali-activated blast-furnace slag pastes and the nature of the calcium silicate hydrate (C–S–H) phase. Cem Concr Res 1994;24:813–29.

[31] Richardson IG, Groves GW. The incorporation of minor and trace elements into calcium silicate hydrate (C–S–H) gel in hardened cement pastes. Cem Concr Res 1993;23:131–8.

[32] Harrisson AM, Winter NB, Taylor HFW. An examination of some pure and composite portland cement pastes using scanning electron microscopy with X-ray analytical capability. In: Proceedings of the eighth International Congress Chem. Cem. IV 1986;170–5.

[33] Richardson IG. The structure of C–S–H in hardened slag cement pastes. In Proceedings of the 10th International Congress Chem. Cem. 1997;2:2ii068, 8 p.

[34] Mascolo G, Marino O. MgO-bearing phases in the hydration products of slag cement. Proceedings of the seventh International Congress Chem. Cem. II 1980;III-58–III-62.

[35] Brindley GW, Kikkawa SM. A crystal chemical study of Mg, Al and Ni, Al hydroxy-perchlorates and hydroxy-carbonates. Amer Mineral 1979;64:836–43.

[36] Brydson R, Richardson IG, McComb DW, Groves GW. Parallel electron energy loss spectroscopy study of Al-substituted calcium silicate hydrate (C–S–H) phases present in hardened cement pastes. Solid State Commun 1993;88:183–7.

[37] Richardson IG, Brough AR, Brydson R, Groves GW, Dobson CM. The location of aluminum in substituted calcium silicate hydrate (C–S–H) gels as determined by ^{29}Si and ^{27}Al NMR and EELS. J Am Ceram Soc 1993;76:2285–8.